Journal of Power Sources 450 (2020) 227609

Contents lists available at ScienceDirect

Journal of Power Sources

journal homepage: www.elsevier.com/locate/jpowsour

Novel twin-perovskite nanocomposite of Ba–Ce–Fe–Co–O as a promising triple conducting cathode material for protonic ceramic fuel cells

Zeyu Zhao, Jiang Cui, Minda Zou, Shenglong Mu, Hua Huang, Yuqing Meng, Kai He, Kyle S. Brinkman, Jianhua (Joshua) Tong *

Department of Materials Science and Engineering, Clemson University, Clemson, SC, 29634, USA

HIGHLIGHTS

- A twin-phase perovskite nanocomposite was synthesized by one-pot synthesis.
- The nanocomposite consists of cubic and orthorhombic perovskite phases.
- The nanocomposite has triple conductivity of proton, oxygen ion, and electron.
- The nanocomposite cathode showed promising oxygen reduction reaction performance.

ABSTRACT

A stable twin-perovskite nanocomposite of Ba–Ce–Fe–Co–O was synthesized by a one-pot Pechini synthesis method. This discovery has opened a new avenue in the development of high-performance cathodes for protonic ceramic fuel cells (PCFCs). The symmetrical cells showed relatively low cathode area-specific resistance compared with existing the state-of-the-art PCFC cathodes. The single cells demonstrated a low polarization resistance of 0.075 Ω cm^2 and a high peak power density of 335 mW cm^2 at 700 °C under an Air/H_2 gradient.

1. Introduction

In recent years, intermediate-temperature (300–700 °C) protonic ceramic fuel cells (PCFCs) have demonstrated outstanding performance [1–5] after the discovery of stable and highly conductive electrolyte and the invention of the single cells fabrication technologies at moderate firing temperatures. However, the slow intermediate-temperature oxygen reduction reaction (ORR) kinetics of the current generation of PCFC cathodes has presented the most significant challenges for further improvement of the PCFC performance [6].

Mixed ionic and electronic conducting (MIEC) perovskite oxides were initially studied as cathodes for intermediate-temperature PCFCs because of their well-demonstrated ORR performance for the conventional oxygen ion-conducting solid oxide fuel cells (SOFCs) [7,8]. Although decent ORR activities were obtained in PCFCs, the area-specific resistances (ASRs) of the MIEC cathodes were usually much higher than those working on oxygen ion-conducting SOFCs. Because the involvement of water formation and diffusion in addition to oxygen diffusion and reduction on PCFC cathodes require the triple conduction of oxygen ions, protons, and electrons in order to achieve the best performance [9,10]. The insufficient proton conductivity of the MIEC cathodes makes them intrinsically deficient materials for PCFC cathodes. The mixed protonic and electronic conducting oxides also didn't show promising PCFC cathode performance due to inadequate oxygen ion conductivity [11]. Alternatively, the microcomposite cathodes (Fig. 1a) comprised of protonic conducting (PC) phase and MIEC phase commonly prepared by mechanically mixing crystallized powders can garner the triple conductivity (O^{2-}/H^+/e^-), which significantly improved the PCFC cathode performance [12]. However, the mechanical mixing method usually results in the microsized PC and MIEC phases [13]. The corresponding long (O^{2-}/H^+/e^-) transport paths, low area of active interfaces, and poor two-phase percolation in the microcomposite cathodes inevitably make it difficult to improve the cathode performance further. Also, the microcomposite cathodes prepared by the mechanical mixing method usually are not under thermodynamic equilibrium, which drives the sluggish solid-state reaction to form new interface impurities, emergent phase [14] or slow adjustment of phase composition resulting in ORR performance degradation. The infiltration is another promising method to further improve the performance of cathodes [15,16]. Interfaces between the infiltrated phase and electrode

* Corresponding author.
E-mail address: jianhut@clemson.edu (J. Tong).

https://doi.org/10.1016/j.jpowsour.2019.227609
Received 27 September 2019; Received in revised form 10 December 2019; Accepted 11 December 2019
Available online 23 December 2019
0378-7753/

scaffold were significantly modified by well contact. However, the coarsening, structure degradation and other problems are still challenges for application [17]. Laterly, a significant improvement of the PCFC ORR kinetics was obtained by the development of phase-pure triple conducting oxide cathodes through heavily doping PC perovskite oxides with transition metals such as Fe, Co, and Ni [2,18]. The discovery of the new triple conducting oxide cathode materials attracted increasing attention because the whole surface of the cathode is activated for ORR [9]. However, the confinement of multiple elements in one crystal structure (e.g., Ba, Co, Fe, Zr, Y in a cubic perovskite structure) significantly limited the further discovery of new triple conducting oxide cathode materials using the same doping strategy. Furthermore, fundamental physical constraints on the coexistence of proton and electron/oxygen ion conductivities is still a significant hinder for freely adjusting the triple conductivities in the phase-pure compound [19].

Most recently, a composite membrane with a nominal composition of $BaCe_{0.5}Fe_{0.5}O_{3-\delta}$ was obtained by one-pot synthesis and was identified to comprise of PC phase of $BaCe_{0.85}Fe_{0.15}O_{3-\delta}$ and MIEC phase of $BaCe_{0.15}Fe_{0.85}O_{3-\delta}$ [20]. The high hydrogen permeability was achieved because of the coexistence of proton and electron conductivities in different phases. Motivated this work, by avoiding the weakness of the state-of-the-art PCFC cathodes, as shown in Fig. 1b, we designed and fabricated a twin-perovskite nanocomposite cathode (TPNCC) comprised of PC and MIEC nanophases. The TPNCCs have the potential to independently adjust the PC and MIEC phase composition for achieving the desired triple conductivities. Compared with microcomposite cathodes, the TPNCCs have shorter transport paths for the charged species and higher active interface concentration between PC and MIEC phases [21]. Furthermore, the one-pot Pechini synthesis method was used to form stable well-percolated PC and MIEC nanocomposites, which can further garner the cathode stability and activity. In this work, the Ba–Ce–Fe–Co–O (BCFC) TPNCC, with a nominal composition of $BaCe_{0.4}Fe_{0.4}Co_{0.2}O_{3-\delta}$, achieved PCFC cathode performance comparable to the highest state-of-the-art ones, which successfully proved the designed TPNCC concept (Fig. 1b) for opening a new avenue toward to the high-performance PCFC cathodes.

2. Experimental

2.1. Chemicals

Barium carbonate ($BaCO_3$, 99.8%), barium nitrate ($Ba(NO_3)_2$,99+%), cerium nitrate hexahydrate ($Ce(NO_3)_3{\cdot}6H_2O$, 99.5%), cobalt (II) nitrate hexahydrate ($Co(NO_3)_3{\cdot}6H_2O$, 98–102%), ethylenediaminetetraacetic acid (EDTA, 99.4%), iron (III) nitrate nonahydrate ($Fe(NO_3)_3{\cdot}9H_2O$, 98+%), cerium oxide (CeO_2, 99.9%), nickel (II) oxide (NiO, Ni-base 78.5%), ytterbium (III) oxide (Yb_2O_3, 99.9%), yttrium (III) oxide (Y_2O_3, 99.9%), zirconium (IV) oxide (ZrO_2, 99.7%), isopropanol (IPA, 70% v/v), and 1-butanol were purchased from Alfa Aesar. The starch (practical grade) was purchased from Sigma Aldrich. The alpha-terpineol (97+%), and citric acid monohydrate (99.5%) were purchased from ACROS Organics. The ammonium hydroxide ($NH_3{\cdot}H_2O$, 28–30% w/w) was purchased from LabChem. The V-600 was purchased from the Heraeus company. The solsperse 28000 was obtained as a sample from the Lubrizol company. All chemicals were used as received without further purification.

2.2. Preparation of $BaCe_{0.4}Fe_{0.4}Co_{0.2}O_{3-\delta}$ (BCFC) precursor powder

BCFC precursor powders were synthesized by a modified Pechini method. Stoichiometric amounts of $Ba(NO_3)_2$, $Ce(NO_3)_3{\cdot}6H_2O$, $Fe(NO_3)_3{\cdot}9H_2O$, $Co(NO_3)_3{\cdot}6H_2O$ were dissolved into deionized water. EDTA and citric acid were added at a mole ratio of 1.5: 1.5: 1 for EDTA: citric acid: total metal ions under magnetic stirring condition. $NH_3{\cdot}H_2O$ was then added to dissolve salts totally by adjusting pH value around 10. The clear solute was heated to 80–90 °C to evaporate the water for forming a viscous gel. The gel was dried in a box oven at 150 °C for 48 h to form a dark charcoal-like primary powder, which was then fired at 600 °C for 5 h followed by ball milling for 7 days in 1-butanol. The cathode precursor powders were obtained by solvent filtration followed by further drying at 500 °C for 5 h. The cathode precursor powders were further ball-milled in isopropanol for the preparation of cathode paste.

2.3. Preparation of precursor powders of anodes and electrolytes

Precursor powders of anodes and electrolytes were prepared by a mechanically mixing raw material powders by ball milling in isopropanol followed by oven drying. Using the electrolyte $BaCe_{0.7}Zr_{0.1}Y_{0.1}Yb_{0.1}O_{3-\delta}$ (BCZYYb) + 1 wt% NiO precursor powder as an example, the preparation can be described as follow. Proper amounts of $BaCO_3$, CeO_2, ZrO_2, Y_2O_3, and Yb_2O_3 in stoichiometry ratio of BCZYYb and additional 1 wt% NiO as a sintering aid was ball-milled for 48 h with 3 mm yttria-stabilized zirconia balls grinding media and isopropanol as grinding solvent. The slurry was then heated at 150 °C in a box oven for 48 h to get fully dried. Anode BCZYYb +65 wt% NiO+ 20 wt% starch was prepared by mixing with $BaCO_3$, CeO_2, ZrO_2, Y_2O_3 Yb_2O_3, 65 wt% NiO and extra 20 wt% starch using the same procedure.

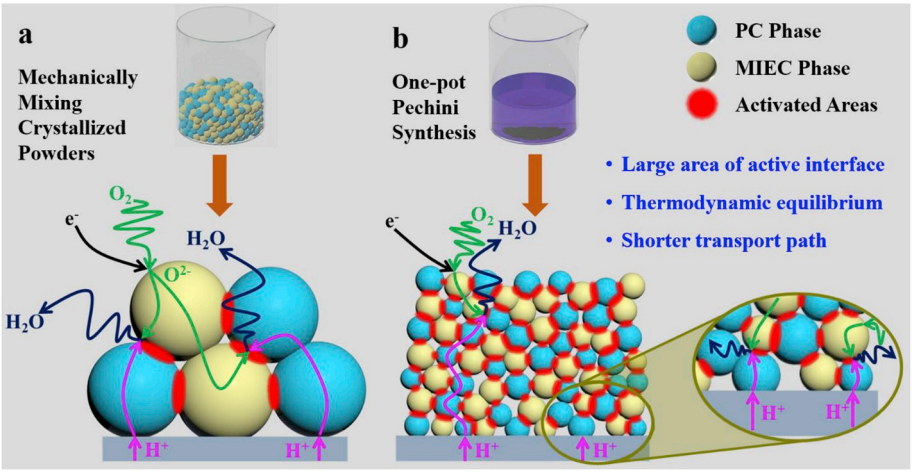

Fig. 1. Schemes of preparation, phase structure, interface area, and reactions of (a) microcomposite cathodes and (b) twin-perovskite nanocomposite cathodes, respectively. PC: protonic conducting; MIEC: mixed ionic and electronic conducting.

2.4. Preparation of electrolyte and cathode precursor pastes

Pastes of electrolyte and cathode precursors were prepared according to the following procedure. The mixture consisting of precursor powder, dispersant (20 wt% solsperse 28000 in terpineol solution), and binder (5 wt% V-600 in terpineol solution) in a weight ratio of 15:3:1 was mixed by manually grinding for 45 min in an agate mortar with an agate pestle.

2.5. Preparation of BCFC pellets for composition identification

The BCFC green pellets were prepared as the following procedure. BCFC precursor powders were firstly calcined at 900 °C for 5 h, then dry-pressed under 350 MPa for 120 s in circular carbon-aided steel die set, which have a diameter of 19 mm and a thickness of ~1 mm. Subsequently, the green pellets were sintered at 1200 °C for 12 h.

2.6. Fabrication of symmetrical cells

Symmetrical cells were fabricated in the electrode | electrolyte | electrode configuration. The BCZYYb electrolyte pellets were fabricated by the solid-state reactive sintering method described as follows. The BCZYYb + 1 wt% NiO electrolyte precursor powders were pressed into green pellets under 350 MPa for 120 s in the circular carbon-aided steel die set. The green electrolyte pellets have a diameter of 19 mm and a thickness of ~2 mm. After sintering at 1450 °C for 18 h, the BCZYYb electrolyte pellets were obtained. After that, the cathode precursor paste was screen printed on both sides of the polished electrolyte pellets and then annealed at 800°C–950 °C for 5 h. Silver mesh and gold wire were attached to the electrode surfaces to work as current collectors and mechanical support lead wire. Ag paste was also applied as electrodes to make symmetrical cells for comparison.

2.7. Fabrication of single cells

The anode green pellets were obtained by dry-pressing under 350 MPa for 120 s in circular carbon-aided steel die set, which has a diameter of 19 mm and a thickness of ~2 mm. Electrolyte layers were applied on both sides of green anode pellets by screen-printing method, followed by firing at 1450 °C for 18 h. Fired pellets were polished to remove extra electrolyte layer and were screen-printed with BCFC paste (~20 μm) of 12 mm in diameter on the electrolyte layer. Subsequently, the whole structure was fired at 900 °C for 5 h. Single cells in porous anode | dense electrolyte | porous cathode structures were obtained. Silver mesh and gold wire worked as current collectors, attached to the electrode surfaces using silver paste.

2.8. Characterization

Microstructures were characterized by scanning electron microscopy (SEM) of a Hitachi S-4800 microscope. A Rigaku Ultima IV diffractometer using monochromatic Cu Kα radiation was utilized to record the powder X-ray diffraction (XRD) patterns. The phase structure was further investigated by high-resolution transmission electron microscopy (HRTEM) of a Hitachi H-9600 microscope. And the element composition was detected by the Energy Dispersive X-Ray Spectroscopy (EDX) (Oxford) component on S-4800.

Symmetrical cells were measured by a Gamry Reference 600 Plus Potentiostat electrochemical impedance spectra (EIS) over a range of temperatures 300°C–700 °C under wet flowing air (through room-temperature water bubbler, 50 mL min^{-1}), using a signal amplitude of 10 mV in the frequency range of 0.01 Hz–5 MHz. The results obtained from EIS were further analyzed with ZView software. The single-cell performance was taken by a Gamry Reference 3000 with cyclic voltammetry, Potentiostat EIS, and open-circuit voltages (OCVs).

3. Results and discussion

The BCFC powders were synthesized by a one-pot Pechini method, and XRD was employed to study the phase composition of BCFC powders with different calcination temperatures. Fig. S1 shows that, before the calcination, the precursor powder pretreated at 500 °C mostly consists of $BaCO_3$ and amorphous phases. All the calcined specimens exhibit almost identical XRD patterns except for the minor carbonate impurity and amorphous impurity in the sample calcined at 800 °C. These XRD patterns can be reasonably indexed as two distinct perovskite phases. The Rietveld refinement analysis of the XRD patterns (Fig. S2) of the BCFC sample calcined at 900 °C indicates that the BCFC composite consists of a cubic perovskite ($Pm\bar{3}m$) phase and an orthorhombic perovskite ($Pbnm$) phase with a ratio of about 4:1. The lattice parameters of the two phases obtained by the same refinement procedures for the specimens calcined at temperatures of 800°C–950 °C are shown in Table S1. It reveals that the lattice parameters are independent of the calcination temperature. Furthermore, the HRTEM was used to identify the morphology and crystal structures of the BCFC powders. Fig. 2a indicates that the nanograins are interlocked into a nanocomposite framework. The selected area electron diffraction (SAED) pattern (Fig. 2b) obtained from this region displays the polycrystalline diffraction rings of the BCFC composite, which is further converted into the intensity profile displayed as a radial average shown in Fig. 2c. It is evident that all SAED peaks are consistent with those acquired from XRD and indicate a clear separation between the cubic (110) and orthorhombic (112) reflections, confirming the successful fabrication of the TPNCs. Furthermore, the HRTEM image taken from two overlapped grains (Fig. 2d) reveals the atomic structures of the two perovskite phases, in which the cubic (110) lattice distance of 0.288 nm and the orthorhombic (112) lattice distance of 0.307 nm are clearly resolved. The enlarged HRTEM images of both phases and the corresponding fast Fourier transform (FFT) patterns are displayed in Fig. 2f-i, respectively. By applying FFT filters on the characteristic reciprocal reflections and coding with pseudo colors, the cubic BCFC grain (shown in purple) and the orthorhombic BCFC grain (shown in green) can be visually identified separately, as illustrated in Fig. 2e. Overall, the TEM characterization elucidates that the TPNCCs composed of cubic and orthorhombic grains are uniformly distributed in the fabricated specimen, while the nanograins of these two phases are locally coupled together in the close vicinity to each other.

It is a problematic process to quantify the elemental composition of each phase in the intergrown nanograins shown in Fig. 2 limited by the resolution of the EDX. Moreover, the porous structure is not suitable for the mapping detection due to the geometry effect on accuracy. In order to get a rough idea about the elemental composition of each phase in the BCFC nanocomposite, the large-grain composite BCFC pellets were prepared at 1200°C for 12h and occupied for both point and mapping quantifications. The area and positions used for analysis were shown in Fig. S3 and the average amount of each element in different phases were presented in Table 1. Based on this result, the element amount of the large-area composite was similar to the theoretical amount we designed, considering the accuracy of EDX quantification. However, for each perovskite phase, the pellet was sintered at 1200 °C which is much higher than the calcination temperature of the cathode layer. The element composition may change due to the temperature increasing. Only the tendency could be concluded from this result that the orthorhombic is a Ce-rich phase and the cubic phase is a Fe-rich phase.

Typically, the PCFC cathode performance is strongly dependent on the cathode morphologies governed by the cathode preparation temperatures. Symmetrical cells of BCFC | BCZYYb | BCFC were prepared at temperatures from 800 to 950 °C to optimize the morphology for achieving the best cathode ASRs. The ASRs of the symmetrical cells were measured using EIS at different temperatures from 300 °C to 700 °C, which are displayed in Fig. S4. Obviously, these four specimens could be

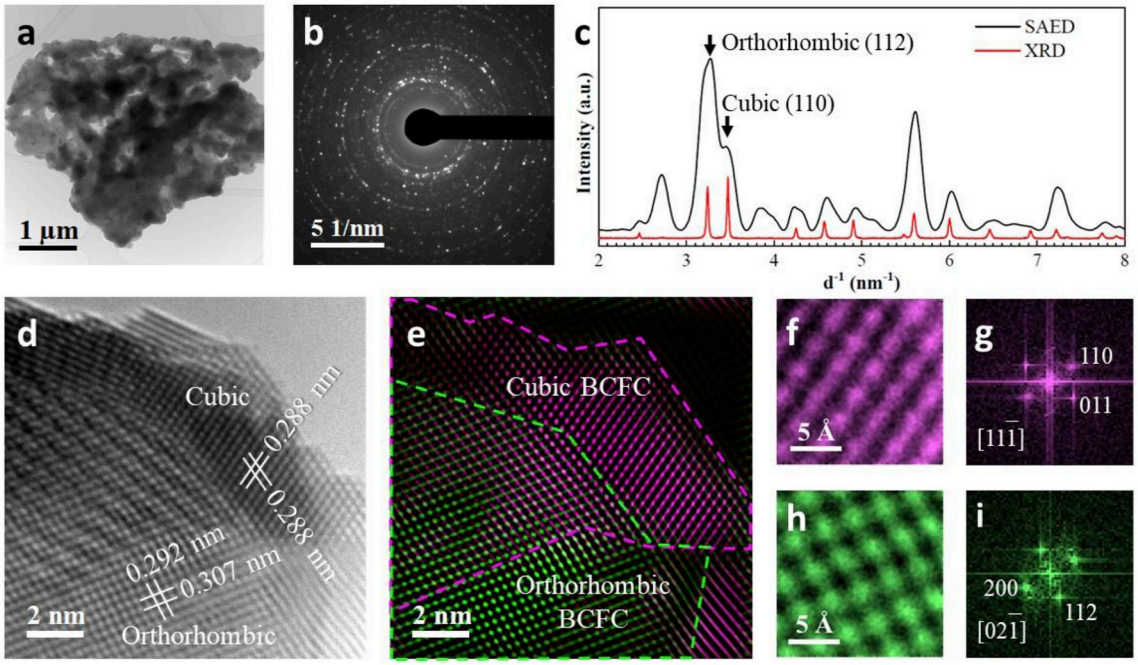

Fig. 2. Structure characterization of BCFC prepared at 900 °C: (a) TEM image and (b) selected-area electron diffraction (SAED) pattern of as-prepared BCFC nanocomposites. (c) radially averaged intensity profile of the SAED shown in (b) as compared to the XRD pattern to indicate the coexistence of cubic and orthorhombic perovskite phases. (d) the HRTEM image of BCFC nanocomposite grains in cubic and orthorhombic perovskite phases. (e) FFT-filtered HRTEM image obtained from (d) to show the overlap of cubic perovskite (purple) and orthorhombic perovskite (green) grains outlined by the dashed lines. (f) enlarged HRTEM image and (g) the corresponding FFT reflections of the cubic BCFC grain in (d). (h) enlarged HRTEM image and (i) the corresponding FFT reflections of the orthorhombic BCFC grain in (d). (For interpretation of the references to color in this figure legend, the reader is referred to the Web version of this article.)

Table 1
Element molar percentage for BCFC pellet sintered at 1200 °C (Normalized numbers based on Ba amount were shown in brackets).

Phase	Ba	Ce	Fe	Co
Large Area	51.28%	18.97%	20.00%	9.75%
Composite	(1.00)	(0.37)	(0.39)	(0.19)
Orthorhombic	51.55%	30.41%	11.86%	6.18%
Perovskite	(1.00)	(0.59)	(0.23)	(0.12)
Cubic Perovskite	51.02%	12.76%	24.49%	11.73%
	(1.00)	(0.25)	(0.48)	(0.23)

classified into two groups: the samples calcined at 800°C–900 °C (group 1) and the samples calcined at 950 °C (group 2). For group 1, the ASRs decreased gradually with increasing the calcination temperature. By further increasing the calcination temperature to 950 °C, larger ASRs were obtained in most of the test temperature range compared with the other three samples. Based on the activation energy calculated from ASR plots, the ASR plots could be separated into a high-temperature range (450–700 °C) and a low-temperature range (300–450 °C). For group 1, the activation energies in the high-temperature range increased with increasing the calcination temperature. The absolute activation energy values of 0.71–0.84 eV are comparable or even lower than the phase-pure triple conducting oxide cathodes, while the group 2 displayed a higher value of 1.46 eV. In the low-temperature range, the samples in group 1 exhibited higher activation energies around 1.37–1.46 eV, which might result from the insufficiently activated grain boundary conduction and the oxygen-ion conductivity causing a blockage of conducting pathways inside the cathode. Similarly, the group 2 displayed activation energy of only 0.98 eV. Overall, the cathode prepared at 900 °C exhibited the lowest ASRs at the studied temperature range. Fig. S5 provides the SEM images of these four BCFC cathodes made at 800–950 °C. The samples in group 1 are all comprised of nanosized grains, while the one made at 950 °C shows obviously larger grain size, which may contribute to the abnormal phenomenon discussed above. The detailed observation indicates that the sample calcined at 900 °C has a better inter-grain connection than the other three samples, which garnered the better percolation of the twin-perovskite phase, the prerequisite of the excellent ORR performance.

The performance of the BCFC cathode prepared at 900 °C was further tested in the anode supported PCFC single cells under the H_2/Air gradient. Fig. 3a provides the I–V and I–P curves of the single-cell at 600 °C–700 °C under the H_2/air gradient. The open-circuit voltages (OCVs) of the single cells are 1.036 V, 1.070 V, and 1.097 V at 700 °C, 650 °C, and 600 °C, respectively, which are close the theoretical OCV values at these temperatures, indicating the good single cell sealing and negligible electrolyte electronic leak. Consistent with most of the other PCFCs, the power density of our BCFC cathode based single cells monotonically increases with increasing the temperature. The peak power densities are 335, 287 and 237 mW cm^2 at 700 °C, 650 °C, and 600 °C respectively. The corresponding current densities are 612 mA cm^{-2}, 507 mA cm^{-2}, and 421 mA cm^{-2}, respectively. Fig. S6a presents the EIS spectra recorded on BCFC cathode based single cells at different temperatures. All spectra were fitted with the equivalent circuit (inset in Fig. S6b) by ZView software. The total single-cell ASR (R_T), the ohmic ASR (R_O), and the polarization ASR (R_P) are plotted in Fig. 3b as a function of the temperature. With increasing the temperature from 600 °C to 700 °C, both the R_O and R_P decreased obviously, in which R_P decreased from 0.263 Ω cm^2 to 0.075 Ω cm^2, and the R_O decreased from 0.92 Ω cm^2 to 0.65 Ω cm^2. Based on the electrolyte thickness of 70 μm, the conductivities of the electrolyte layer are 0.0154 S cm^{-1}, 0.0176 S cm^{-1} and 0.0219 S cm^{-1} at 600 °C, 650 °C and 700 °C, respectively, which are close to the values at corresponding temperatures (0.0140 S cm^{-1}, 0.0189 S cm^{-1} and 0.0258 S cm^{-1}) for the BCZYYb pellets synthesized by solid state reactive sintering method. Thus, it is reasonable to conclude that large ohmic resistance was related to the big thickness of the electrolyte layer. Furthermore, the R_P only occupies 10–20% of the total ASR of the single cells, which means that the R_O is responsible for the main resistance during the operation due to

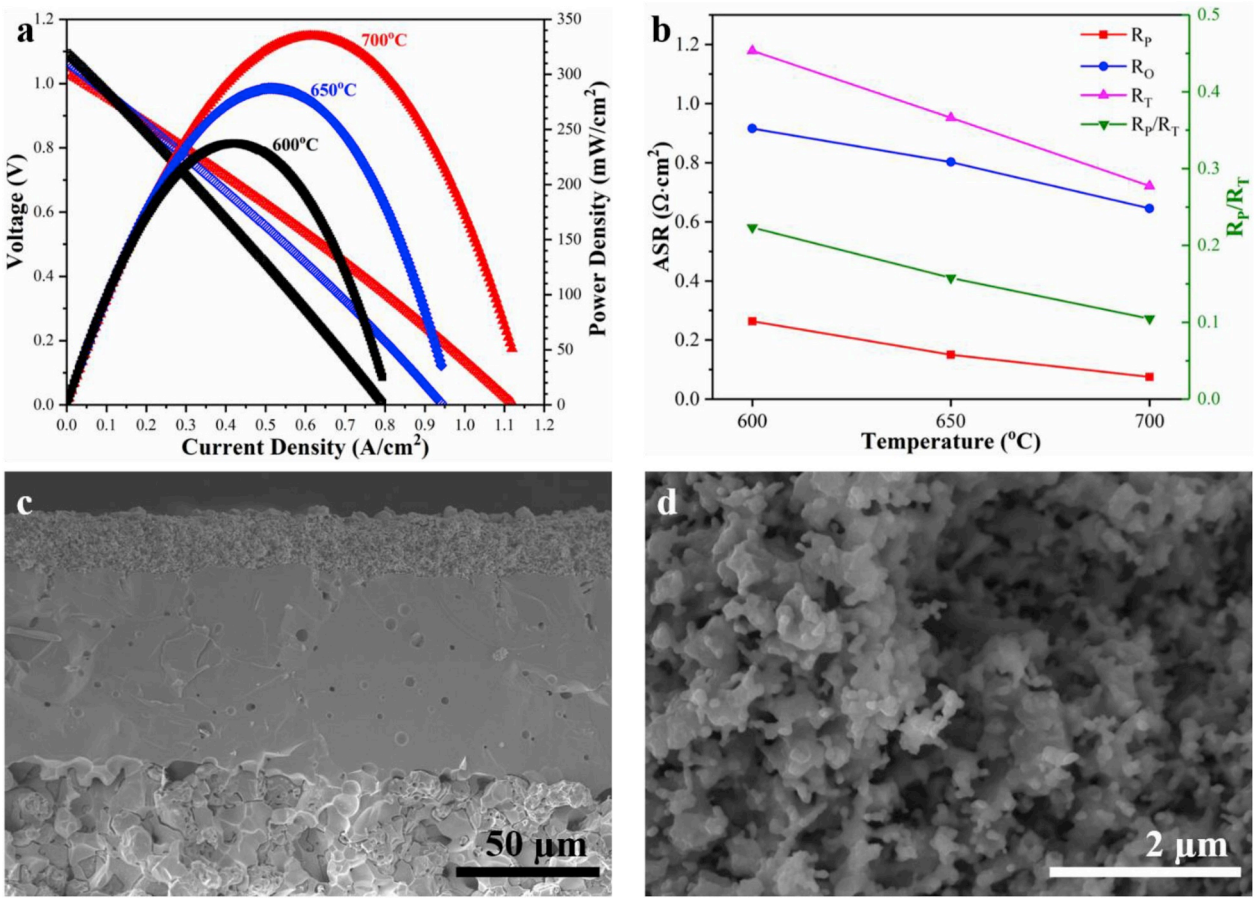

Fig. 3. BCFC cathode calcined at 900 °C: (a) I–V and I–P curves of single-cell measured under a dry hydrogen atmosphere at different temperatures. (b) the polarization resistances, ohmic resistances, and total resistances determined from the EIS. (c) the cross-sectional morphology of a PCFC single cell after testing. (d) the cross-sectional view of the BCFC cathode.

~70 μm of thickness, and there is still more space to improve the single performance in the future. Furthermore, it should be mentioned the R_P values reported here are the sums of both anode and cathode, which means that the ASRs of our BCFC TPNCC should be smaller than the 0.075 Ω cm^2 and 0.263 Ω cm^2 at 700 °C and 600 °C respectively. Fig. 3c&d shows the morphology of the cross-section images of single cells after the performance test at temperatures from 600 to 700 °C. It is clear that the adherence between BCFC cathode and BCZYYb electrolyte is still firm, and the morphology of the BCFC is still the same as the as-fabricated BCFC cathode.

The performance of our BCFC TPNCC was compared with the state-of-the-art PCFC cathode based on the symmetrical cell ASRs measured by EIS under wet flowing air. Fig. 4 summarized the ASRs of more than 50 state-of-the-art PCFC cathodes, including MIEC, mixed protonic and electronic conducting, microcomposite, triple conducting oxide cathodes. Obviously, our twin-perovskite nanocomposite cathode of BCFC shows relative lower ASR values for 400–700 °C than most of the listed cathodes, the superior PCFC cathode performance. It should be noted that the ASR values in Fig. 4 were obtained from different electrolytes. Only the tendency is meaningful rather than the exact values [22]. The stability of our BCFC TPNCC was further studied by monitoring the ASR of symmetrical cells at 700 °C in air. Fig. S7 indicates that the ASR does not show noticeable degradation within 50 h, which preliminarily proves that our new BCFC TPNCC is relatively stable. Considering the highest operating temperature for intermediate-temperature PCFC is not higher than 650 °C, the newly developed BCFC TPNCC should be a stable cathode for intermediate-temperature PCFCs.

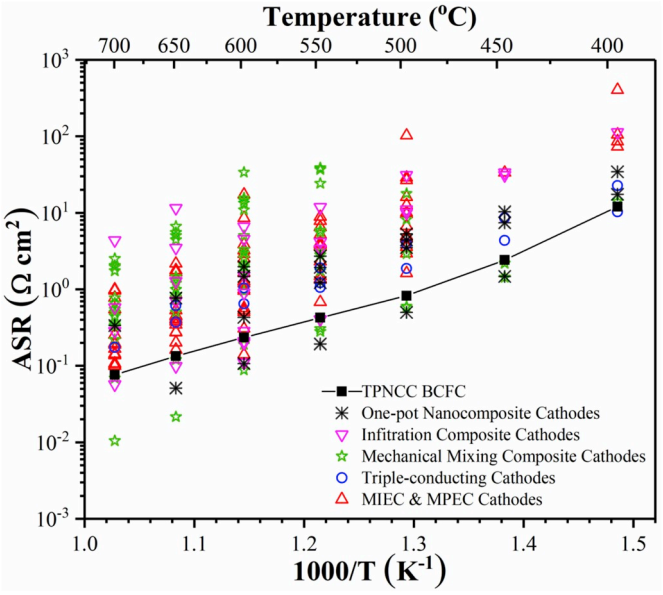

Fig. 4. ASR values of representative cathodes tested as symmetric cell formation under wet air atmosphere. (The whole list of cathode materials can be found in Table S1).

4. Conclusions

In this work, a tripe conducting ($O^{2-}/H^{+}/e^{-}$) twin-perovskite nanocomposite cathode (TPNCC) based on a nominal composition of $BaCe_{0.4}Fe_{0.4}Co_{0.2}O_{3-\delta}$ was designed and fabricated by the one-pot Pechini synthesis method. XRD, SEM, and HRTEM confirmed the formation of the nanocomposites comprised of cubic perovskite phase and orthorhombic perovskite phase. The interlocked perovskite nanograins make it not trivial for the identification of the actual compositions of each perovskite phase, which in fact, is under investigation in our laboratory. The testing of PCFC symmetrical cells demonstrated that BCFC TPNCC has a relatively lower ASR of 0.075 $\Omega\,cm^2$ at 700 °C compared with most of the state-of-the-art PCFC cathodes. The PCFC single-cell testing achieved peak power densities of 335, 287, and 237 mW cm^2 at 700, 650, and 600 °C, respectively, which can be further improved by optimizing the electrolyte since the total electron polarization contribution the single-cell resistance is only 10–20%. These results indicated that the TPNCCs have the great potential to open a new avenue toward to the high-performance PCFC cathodes. The stable twin-perovskite nanocomposites with independently adjustable conductivity in each individual phase can provide new candidate materials for energy conversion and storage technologies.

Disclaimer

"This report was prepared as an account of work sponsored by an agency of the United States Government. Neither the United States Government nor any agency thereof, nor any of their employees, makes any warranty, express or implied, or assumes any legal liability or responsibility for the accuracy, completeness, or usefulness of any information, apparatus, product, or process disclosed, or represents that its use would not infringe privately owned rights. Reference herein to any specific commercial product, process, or service by trade name, trademark, manufacturer, or otherwise does not necessarily constitute or imply its endorsement, recommendation, or favoring by the United States Government or any agency thereof. The views and opinions of authors expressed herein do not necessarily state or reflect those of the United States Government or any agency thereof."

Declaration of competing interest

The authors declare that they have no known competing financial interests or personal relationships that could have appeared to influence the work reported in this paper.

Acknowledgment

This material is based upon work supported by the U.S. Department of Energy's Office of Energy Efficiency and Renewable Energy (EERE) under the Fuel Cell Technologies Office Award Number DE-EE0008428. K.H. acknowledges Clemson University's start-up fund and CU-CIA grant for the use of the Electron Microscopy Facility, which was funded in part by Clemson University's R-Initiative Program.

Appendix A. Supplementary data

Supplementary data to this article can be found online at https://doi.org/10.1016/j.jpowsour.2019.227609.

References

[1] L. Yang, S. Wang, K. Blinn, M. Liu, Z. Liu, Z. Cheng, M. Liu, Enhanced sulfur and coking tolerance of a mixed ion conductor for SOFCs: BaZr(0.1)Ce(0.7)Y(0.2-x)Yb (x)O(3-delta), Science 326 (2009) 126–129, https://doi.org/10.1126/science.1174811.

[2] C. Duan, J. Tong, M. Shang, S. Nikodemski, M. Sanders, S. Ricote, A. Almansoori, R. O'Hayre, Readily processed protonic ceramic fuel cells with high performance at low temperatures, Science 80 (2015), https://doi.org/10.1126/science.aab3987.

[3] C. Duan, R.J. Kee, H. Zhu, C. Karakaya, Y. Chen, S. Ricote, A. Jarry, E.J. Crumlin, D. Hook, R. Braun, N.P. Sullivan, R. O'Hayre, Highly durable, coking and sulfur tolerant, fuel-flexible protonic ceramic fuel cells, Nature 557 (2018) 217–222, https://doi.org/10.1038/s41586-018-0082-6.

[4] S. Choi, C.J. Kucharczyk, Y. Liang, X. Zhang, I. Takeuchi, H.-I. Ji, S.M. Haile, Exceptional power density and stability at intermediate temperatures in protonic ceramic fuel cells, Nat. Energy 3 (2018) 202–210, https://doi.org/10.1038/s41560-017-0085-9.

[5] H. An, H.-W. Lee, B.-K. Kim, J.-W. Son, K.J. Yoon, H. Kim, D. Shin, H.-I. Ji, J.-H. Lee, A 5 × 5 cm2 protonic ceramic fuel cell with a power density of 1.3 W cm–2 at 600 °C, Nat. Energy 3 (2018) 870–875, https://doi.org/10.1038/s41560-018-0230-0.

[6] R. Zohourian, R. Merkle, G. Raimondi, J. Maier, Mixed-conducting perovskites as cathode materials for protonic ceramic fuel cells: understanding the trends in proton uptake, Adv. Funct. Mater. 28 (2018), https://doi.org/10.1002/adfm.201801241, 1801241.

[7] A. Grimaud, F. Mauvy, J.M. Bassat, S. Fourcade, L. Rocheron, M. Marrony, J. C. Grenier, Hydration properties and rate determining steps of the oxygen reduction reaction of perovskite-related oxides as H^{+}-SOFC cathodes, J. Electrochem. Soc. 159 (2012) B683–B694, https://doi.org/10.1149/2.101205jes.

[8] Y. Lin, W. Zhou, J. Sunarso, R. Ran, Z. Shao, Characterization and evaluation of BaCo0.7Fe0.2Nb0.1O3−δ as a cathode for proton-conducting solid oxide fuel cells, Int. J. Hydrogen Energy 37 (2012) 484–497, https://doi.org/10.1016/J.IJHYDENE.2011.09.010.

[9] J. Kim, S. Sengodan, G. Kwon, D. Ding, J. Shin, M. Liu, G. Kim, Triple-conducting layered perovskites as cathode materials for proton-conducting solid oxide fuel cells, ChemSusChem 7 (2014) 2811–2815, https://doi.org/10.1002/cssc.201402351.

[10] L. Yang, Z. Liu, S. Wang, Y. Choi, C. Zuo, M. Liu, A mixed proton, oxygen ion, and electron conducting cathode for SOFCs based on oxide proton conductors, J. Power Sources 195 (2010) 471–474, https://doi.org/10.1016/j.jpowsour.2009.07.057.

[11] C. Zhang, H. Zhao, A novel cathode material BaCe0.4Sm0.2Co0.4O3−δ for proton conducting solid oxide fuel cell, Electrochem. Commun. 13 (2011) 1070–1073, https://doi.org/10.1016/J.ELECOM.2011.06.035.

[12] R. Peng, T. Wu, W. Liu, X. Liu, G. Meng, Cathode processes and materials for solid oxide fuel cells with proton conductors as electrolytes, J. Mater. Chem. 20 (2010) 6218, https://doi.org/10.1039/c0jm00350f.

[13] T. Matsui, K. Manriki, K. Miyazaki, H. Muroyama, K. Eguchi, A new oxygen reduction electrocatalyst of barium lanthanide cobaltate for composite cathodes of proton-conducting ceramic fuel cells, J. Mater. Chem. A. 6 (2018) 14188–14194, https://doi.org/10.1039/C8TA04093A.

[14] Y. Lin, S. Fang, D. Su, K.S. Brinkman, F. Chen, Enhancing grain boundary ionic conductivity in mixed ionic–electronic conductors, Nat. Commun. 6 (2015) 6824, https://doi.org/10.1038/ncomms7824.

[15] L. Fan, P.-C. Su, Layer-structured LiNi0.8Co0.2O2: a new triple (H+/O2−/e−) conducting cathode for low temperature proton conducting solid oxide fuel cells, J. Power Sources 306 (2016) 369–377, https://doi.org/10.1016/J.JPOWSOUR.2015.12.015.

[16] Z. Zhang, J. Wang, Y. Chen, S. Tan, Z. Shao, D. Chen, In situ formation of a 3D core-shell and triple-conducting oxygen reduction reaction electrode for proton-conducting SOFCs, J. Power Sources 385 (2018) 76–83, https://doi.org/10.1016/J.JPOWSOUR.2018.03.029.

[17] M. Shah, P.W. Voorhees, S.A. Barnett, Time-dependent performance changes in LSCF-infiltrated SOFC cathodes: the role of nano-particle coarsening, Solid State Ion. 187 (2011) 64–67, https://doi.org/10.1016/j.ssi.2011.02.003.

[18] M. Shang, J. Tong, R. O'Hayre, A promising cathode for intermediate temperature protonic ceramic fuel cells: BaCo0.4Fe0.4Zr0.2O3−δ, RSC Adv. 3 (2013) https://doi.org/10.1039/c3ra41828f, 15769.

[19] A. Zhu, G. Zhang, T. Wan, T. Shi, H. Wang, M. Wu, C. Wang, S. Huang, Y. Guo, H. Yu, Z. Shao, Evaluation of SrSc0.175Nb0.025Co0.8O3-δ perovskite as a cathode for proton-conducting solid oxide fuel cells: the possibility of in situ creating protonic conductivity and electrochemical performance, Electrochim. Acta 259 (2018) 559–565, https://doi.org/10.1016/J.ELECTACTA.2017.11.037.

[20] S. Cheng, Y. Wang, L. Zhuang, J. Xue, Y. Wei, A. Feldhoff, J. Caro, H. Wang, A dual-phase ceramic membrane with extremely high H2Permeation flux prepared by autoseparation of a ceramic precursor, Angew. Chem. Int. Ed. 55 (2016) 10895–10898, https://doi.org/10.1002/anie.201604035.

[21] A.M. Abdalla, S. Hossain, A.T. Azad, P.M.I. Petra, F. Begum, S.G. Eriksson, A. K. Azad, Nanomaterials for solid oxide fuel cells: a review, Renew. Sustain. Energy Rev. 82 (2018) 353–368, https://doi.org/10.1016/J.RSER.2017.09.046.

[22] R. Strandbakke, V.A. Cherepanov, A.Y. Zuev, D.S. Tsvetkov, C. Argirusis, G. Sourkouni, S. Prünte, T. Norby, Gd- and Pr-based double perovskite cobaltites as oxygen electrodes for proton ceramic fuel cells and electrolyser cells, Solid State Ion. 278 (2015) 120–132, https://doi.org/10.1016/j.ssi.2015.05.014.